Comparisons of Localized Convection due to Localized Forcing and to Preconditioning

FIAMMETTA STRANEO AND MITSUHIRO KAWASE

School of Oceanography, University of Washington, Seattle, Washington

(Manuscript received 14 July 1997, in final form 26 February 1998)

ABSTRACT

Although observations indicate that localization of deep convection results from oceanic preconditioning and only to a lesser extent from the gradients in the atmospheric forcing, most laboratory and numerical simulations of oceanic deep convection localize convection via the buoyancy forcing. It is as yet unclear to what extent the localized forcing simplification is representative of realistic preconditioned convection and whether conclusions drawn from analyzing the former scenario can be applied to the latter. Comparison between these two localized convection scenarios is the focus of this study. The analysis is conducted using a high-resolution, nonhydrostatic numerical model that assumes no variations in the latitudinal direction. Although this model cannot represent baroclinic instability, it represents well the violent mixing phase of chimney formation that precedes baroclinic instability. Because of the inherently different initial and boundary conditions, there is no single comparison to be made between the two scenarios; all of the comparisons, however, show that a localized forcing tends to enhance the frontal structures at the edge of the convected water mass. The authors explain these results by means of some simple analytical calculations that indicate that convection as a result of a localized forcing induces a continuous increase in the horizontal density gradient, while convection in a surface-intensified, cyclonic gyre results in a decrease in the horizontal gradient. The authors conclude that the two scenarios are not equivalent and discuss how some of the conclusions, valid for localized forcing, do not necessarily apply to the preconditioned scenario. In particular, the equilibrium state observed in localized forcing simulations, in which the lateral fluxes due to the baroclinic eddies balance the surface buoyancy loss, may not have an analog for the case of preconditioned convection.

1. Introduction

In general, poleward of 24°N the ocean loses heat to the atmosphere (Bryden 1993), yet there are very few regions in the world's ocean where this surface buoyancy loss is sufficient to drive deep convection. This resistance to overturning results from the joint action of the ocean's vertical stratification and of the Coriolis force, both acting to inhibit vertical motions so that, even in the few regions where it has been observed, it only occurs over a limited area. The size of the observed convective structures, the chimneys, ranges from 50 km in the Labrador Sea (Gascard and Clarke 1983) to about 60–100 km in the Mediterranean Sea (Leaman and Schott 1991) and 80 km in the Greenland Sea (Schott et al. 1993) to 100 km in the Weddell Sea (Muench 1988). This localization must result from a localized surface buoyancy loss, from the presence of some large-scale structure in the ocean, or from a combination of both. In other words, if this scale is not in the forcing, it must be in the state of the ocean before the convection begins. Since the atmospheric scales, which control the surface buoyancy loss, are typically one order of magnitude larger [O(500 km)] than these chimneys, it follows that this localization must be imparted by the ocean.

Localized convection can be thought of as a nonuniform mixed layer deepening and, given a spatially constant buoyancy flux, there are two parameters that govern the depth to which convection occurs: the vertical stratification and the time over which the buoyancy loss persists. Either an isolated region of weaker stratification or trapping of fluid (so as to expose it to prolonged cooling) would result in localized convection and an area that presents any of these features is then *preconditioned* to deep convection. Such a *preconditioning*, in the ocean, can result from a variety of mechanisms. Among the first to propose a preconditioning mechanism that would then lead to the formation of a convective chimney were Swallow and Gaston (1973) and Hogg (1973) for the northwest Mediterranean. More recently, mechanisms for preconditioning for a number of regions prone to deep convection have been examined in a series of numerical studies. Madec et al. (1996) show that in the northwest Mediterranean it is caused by the formation of a wind-driven barotropic cyclonic gyre in a region of strong buoyancy loss. Advection of lighter fluid into and around the gyre is topographically controlled and results in the trapping of some fluid above

Corresponding author address: Fiammetta Straneo, School of Oceanography, University of Washington, Box 357940, Seattle, WA 98195-7940.
E-mail: fiamma@ocean.washington.edu

the Rhone Deep Sea Fan, where the densest water forms as a result of continuous cooling. In the Weddell Sea, Alverson and Owens (1996) show that preconditioning can result from trapping of fluid over Maud Rise. In their experiments, a constant inflow into the region of cooling results in the formation of a Taylor column over the rise. The stratification of the fluid within the column is progressively eroded during the winter, until a violent cooling event can cause deep convection. In the Labrador Sea, and probably in other regions of the World Ocean, deep convection is thought to occur in drifting cyclonic eddies (Legg et al. 1998), and the preconditioning results from the doming isopycnals within the gyre, causing dense water, with reduced stratification, to be closer to the surface.

Because of its localized and rapid nature, observations of deep convection remain very arduous and sparse. At the same time, there has been a growing demand for adequate parameterizations of oceanic deep convection that can be included in global circulation models, given the paramount importance the thermohaline circulation plays in driving the deep ocean. For these reasons numerical and laboratory simulations of open-ocean deep convection have been extremely valuable in supplementing observations and in trying to determine a series of nondimensional parameters and scaling laws summarizing the integral effects of deep convection. Among the first simulations to address the formation and collapse of a chimney are the laboratory experiments of Maxworthy and Narimousa (1994) and the numerical ones of Jones and Marshall (1993). In both cases the chimney is formed by extracting buoyancy over a disk at the surface of a horizontally homogeneous ocean. Since then, a number of increasingly complex laboratory and numerical experiments have been conducted to provide a better understanding of the formation and collapse of a chimney in a rotating stratified ocean [see, e.g., Visbeck et al. (1996) for a review]. Investigators find that in the initial stages small convective cells, or plumes, act to mix the water column vertically while a surface buoyancy loss induces gravitational instability in the water column. Plumes measure about one kilometer in diameter, and thus have aspect ratio of order one, are somewhat influenced by rotation and have lifetimes that span from hours to days. Since the surface forcing is limited to a finite area in these simulations, it imposes a horizontal density contrast between the modified and unmodified fluid. This horizontal gradient is balanced by a geostrophic rim current resulting in cyclonic circulation at the surface and anticyclonic at depth. Meanders develop as the current becomes baroclinically unstable and may detach in the form of eddies. These eddies are then responsible for the export of dense water from the region of active convection and the import of warmer unmodified water. If the surface buoyancy loss persists for a long enough period of time, the lateral heat flux induced by the eddies can balance the surface flux, causing the arrest of the convective deepening within the chimney, as shown by the laboratory experiments of Ivey and Coates (1995), the heton model of Legg et al. (1996), in the scalings of Visbeck et al. (1996), and, most recently, in the restratification arguments of Jones and Marshall (1997).

Almost all of these simulations, however, share a common simplification: that of removing buoyancy over a finite area at the surface of a quiescent, horizontally homogeneous ocean [typically the same *disk of cooling* used in Jones and Marshall (1993)]. From the modeling perspective there are a number of advantages in studying deep convection by spatially restricting the buoyancy flux. It implies that fluid away from the region of cooling is minimally influenced by convection so that the artificially imposed boundaries of a tank, or of the integration domain, have little consequence on the results. Furthermore, starting from a preconditioned ocean implies dealing with the possible instability of the preconditioning structure even before the onset of the cooling, as well as having to cope with convection occurring at the lateral boundaries. Because so much attention has been devoted to studying localization of convection as a result of the localized buoyancy forcing, it is important to understand to what extent these two scenarios are interchangeable. The comparison between convection in a preconditioned ocean versus convection in a horizontally homogeneous ocean subject to a localized buoyancy flux is the focus of this study, with the intention of determining to what extent the mechanisms identified in one case are operating in the other. To do this, we use a high-resolution, nonhydrostatic numerical model, which assumes no variations in the zonal direction, to resolve the details of upright convection in the presence of horizontal gradients either in the initial density distribution or in the forcing. Although this model cannot represent baroclinic instability, which is responsible for the final collapse of the dense water mass, it enables us to view other processes that play a role in the redistribution of mass and buoyancy and are typically masked by the variability produced by the baroclinic eddies. In addition, we make use of a simpler, one-dimensional mixed layer model that is only capable of reproducing the initial violent mixing stage of convection. The scope of this study is not to derive a new parameterization of the chimney's formation and breakup, but instead to discuss to what extent the dynamics observed in localized forcing simulations are applicable to a preconditioned convection scenario.

The paper is structured as follows. The model and the experimental configurations used are outlined in section 2. There is no single comparison to be made between these two scenarios, therefore in section 3 we describe the experiments and the results for three different comparisons of the two modes causing localized deep convection. The numerical results are then explained on the basis of a simple analytical calculation for the evolution of the horizontal density gradient within the convected water mass in section 4. Finally, we

summarize our results and discuss their implications for oceanic convection in section 5.

2. Models and experimental design

a. Model description

Two different models are used in this study. The first, a one-dimensional model, can only predict the depth and buoyancy distribution of a vertical column of fluid when a buoyancy flux is specified at the surface. Although a very crude model, it represents well the vigorous stage of convective overturning, as discussed by Haine and Marshall (1998) for example, that somewhat justifies the widespread use of vertical mixing schemes in larger scale models unable to resolve the small convective scales. The second is a high-resolution, nonhydrostatic numerical model, which integrates the Boussinesq equations in a vertical plane since it assumes no zonal variations. It resolves convection although plumes should now be thought of as overturning *tubes* of fluid. Such a model can be extremely useful provided one is aware of its limitations: Since it assumes no variation in the zonal direction, it cannot become baroclinically unstable or resolve any three-dimensional plume–plume interaction process. This means that such a model is not adequate for the study of the chimney collapse as a result of baroclinic instability. On the other hand, the no-zonal variation assumption allows us to conduct experiments at a higher resolution if compared to typical three-dimensional numerical simulations of chimney formation. Furthermore, by removing the variability associated with baroclinic instability, this model is ideal for revealing the role played by two-dimensional processes (e.g., symmetric instability) and studying how they contribute to the horizontal density gradient that baroclinic instability then grows upon. Because convection still needs to be parameterized in most large-scale models, it is important to identify all the active mechanisms for convection to be represented correctly.

In both models, we assume a linear equation of state and only solve for buoyancy, $b(y, z, t)$, with $b = -g\rho'/\rho_0$, where g is the gravitational acceleration, ρ_0 is a reference density, and ρ' is the dynamically active part of the density field. The problem is defined by specifying the initial conditions for buoyancy $b_0(y, z)$, and the surface buoyancy flux $Q(y, t)$ (positive Q meaning a heat flux into the ocean) in both models with the addition of initial conditions for the velocity fields in the two-dimensional model.

1) One-dimensional mixed layer model

In this model convection occurs instantaneously and homogenizes the water column to its point of neutral buoyancy. Although neighboring water columns do not interact, y dependence can be included in a parametric sense since either the initial density field or the buoyancy forcing are y dependent. As buoyancy is removed at the surface, the water column is mixed to a depth $z = -h(y, t)$ such that

$$b(y, z, t) = \begin{cases} \overline{b}(y, t) & \text{for } z \geq -h(y, t) \\ b_0(y, z) & \text{for } z \leq -h(y, t) \end{cases} \quad (1)$$

with a continuous buoyancy boundary condition at the bottom of the mixed layer $\overline{b} = b_0(y, -h(y, t))$. Buoyancy conservation in this model can be written as

$$\overline{b}(y, t)h(y, t) - \int_{-h}^{0} b_0(y, z)\, dz = \int_0^t Q(y, t')\, dt'. \quad (2)$$

One can then solve for the mixed layer depth $h(y, t)$ and derive the mixed layer buoyancy $\overline{b}(y, t)$. For the case of constant background stratification, $b_0(y, z) = N^2 z$, this reduces to Turner's (1973) result:

$$h(y, t) = \left(-\frac{2\int_0^t Q(y, t')\, dt'}{N^2} \right)^{1/2}. \quad (3)$$

2) Nonhydrostatic model description

This model assumes no x variations and integrates the buoyancy equation, the equation for the component of vorticity in the x direction, ξ, and the equation for the alongchannel velocity u. The model uses a staggered grid with buoyancy and the zonal velocity defined at the center of the grid rectangle, the normal component of velocity at the sides, and vorticity and streamfunction at the corners. In the usual notation the model equations are

$$\frac{Du}{Dt} - fv = \nu_v \frac{\partial^2 u}{\partial z^2} + \nu_h \frac{\partial^2 u}{\partial y^2} \quad (4)$$

$$\frac{Db}{Dt} = \kappa_v \frac{\partial^2 b}{\partial z^2} + \kappa_h \frac{\partial^2 b}{\partial y^2} \quad (5)$$

$$\frac{D\xi}{Dt} = f\frac{\partial u}{\partial z} + \frac{\partial b}{\partial y} + \nu_z \frac{\partial^2 \xi}{\partial z^2} + \nu_h \frac{\partial^2 \xi}{\partial y^2}, \quad (6)$$

where

$$\frac{D}{Dt} = \frac{\partial}{\partial t} + v\frac{\partial}{\partial y} + w\frac{\partial}{\partial z}, \qquad v = -\frac{\partial \psi}{\partial z}, \qquad w = \frac{\partial \psi}{\partial y},$$
$$\xi = \nabla^2 \psi.$$

Potential vorticity, $q(y, z, t)$ is calculated as a diagnostic in the model:

$$q(y, z, t) = \frac{\partial b}{\partial y}\frac{\partial u}{\partial z} + \frac{\partial b}{\partial z}\left(f - \frac{\partial u}{\partial y} \right). \quad (7)$$

Similarly to other nonhydrostatic simulations of deep convection (Jones and Marshall 1993; Legg et al. 1998) the Prandtl number is chosen to be one and the horizontal diffusivity used is 5 $m^2\ s^{-1}$. Because of the higher

vertical resolution of this model we are able to use a lower vertical diffusivity $\kappa_v = 0.06$ m^2 s^{-1} than was used in these experiments (ranging from 0.2–0.7 m^2 s^{-1}). This value is still large compared to any value estimated by observations but is required for the numerical stability of the model given the comparatively large vertical velocities; nonetheless, this value is small enough not to influence the advection of buoyancy. Horizontal grid spacing is 125 m, while the vertical is 30 m; the basin used is 50 km by 2000 m. Boundary conditions are no flux for buoyancy for the lateral and bottom boundaries, while the flux condition at the surface is given by $Q(y, t) = \kappa_v \partial b/\partial z$. Boundary conditions for the momentum equations are no stress at all boundaries except for the bottom, which is no slip. An Adams–Bashforth time stepping scheme is used with a 60-s time step.

b. Experiment description

There are many forms of preconditioning, as briefly mentioned in the introduction, and here we will concentrate on the simplest one: a region of cyclonic vorticity near the surface subject to uniform surface cooling. In all of the preconditioned experiments a gyrelike structure is superimposed on a background stratification, both decreasing with depth. The cyclonic vorticity acts to reduce the background stratification at its center, and also decays with depth. A similar setup has been utilized by Legg et al. (1998) to study convection in mesoscale eddies. The reduction of the stratification at the center of the gyre exposes denser, weakly stratified fluid, causing convection to occur to a greater depth at the gyre's center. In this idealized study we term *preconditioned experiment* as one in which a spatially uniform buoyancy flux is applied to such a cyclonic vorticity distribution and *localized forcing experiment* as one where a spatially localized buoyancy flux is applied to a quiescent ocean (Fig. 1). Throughout this study, the prefix ''pre'' describes a preconditioned experiment while ''loc'' describes a localized forcing one. The respective initial and boundary conditions can then be formulated as follows:

preconditioned experiment	localized forcing experiment
$b(y, z, t = 0) = b_0(y, z)$	$b(y, z, t = 0) = b_0(z)$
$u(y, z, t = 0) = -\frac{1}{f}\int^z \frac{\partial b_0}{\partial y}(y, z')\, dz'$	$u(y, z, t = 0) = 0$
$w(y, z, t = 0) = 0$	$w(y, z, t = 0) = 0$
$Q(y, t) = Q_0(t)$	$Q(y, t) = Q_0(y, t)$

Parameters for all the experiments listed can be found in Tables 1 and 2. After an initial spinup time the cooling is turned on and applied for a time $t_o = 3.4$ days, comparable to the duration of a typical winter storm that would induce convection. Beyond this time the surface buoyancy flux is switched off and the fluid is left to adjust until day 5. Random noise is superimposed on the initial surface buoyancy field to provide the horizontal gradients for the overturning. Different noise distributions were tested and show that the final state is independent of the initial noise distribution.

3. Comparisons of preconditioned versus localized forcing convection

In adopting the localized forcing scenario to study chimney formation, a number of modelers have claimed its equivalence to preconditioned convection; it is important to understand what *equivalent* means when used to compare these two modes of chimney formation. Ideally, one would like to find that a chimney formed in one scenario is identical to one formed in the other and, if this were true, then it would be reasonable to assume that the collapse and export of dense water would then be the same for both. Alternatively, if the chimneys turn out to be different, one would like to be able to claim that mechanisms observed in one case are also applicable to the other and that, as a result, the scaling laws and parameterizations derived for one scenario can also be adopted for the second. Suppose one had observed a form of preconditioning in the ocean, how can one design a localized forcing simulation that would result in producing a chimney as close to the real one as possible? One needs to identify which parameters govern the chimney's evolution and design the localized forcing experiment where its parameters match those of the observations when appropriately translated into those of the other scenario. In this section we present a series of comparisons in which we have attempted to produce a similar chimney in two different ways. Given the extremely different initial and boundary conditions, we have done this imposing at least one buoyancy-related quantity be the same for both cases. This can be done directly through the boundary conditions, for some

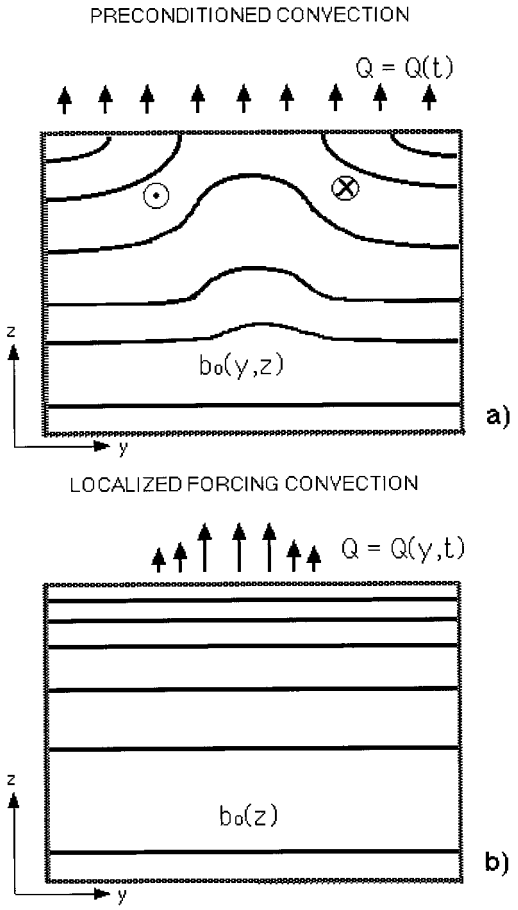

FIG. 1. Schematic of localized convection due to a (a) preconditioned ocean and (b) localized surface buoyancy flux. Solid lines represent b_0, the initial buoyancy distribution, and arrows represent Q, the surface buoyancy flux.

cases, or by assuming some knowledge of the evolution of the fields (e.g., by using the mixed layer model as a predictive tool) and imposing the evolution of some field to be the same in both scenarios.

Three different series of comparison experiments are designed. For each comparison we describe the setup and the results; because some results are common to all three comparisons they are discussed only once but are summarized in the final discussion. In analyzing the results, emphasis is placed on those fields that affect the long-term evolution of the convected water mass and, in particular, to those that are likely to influence the development of baroclinic instability.

a. Comparison of the same spatial dependence and vertically integrated buoyancy content

1) EXPERIMENT DESCRIPTION

A horizontal dependence is needed to localize convection in both scenarios. In experiments pre1 and loc1 we impose the exact same y dependence for $b_0(y, z)$ and $Q(y, t)$, respectively, in the form of a Gaussian with identical e-folding lengths (see Tables 1 and 2). This does not uniquely define the problem, though, and leaves a number of other parameters unspecified. To make the two chimneys as similar as possible the background stratification, the magnitude of the buoyancy flux, and the time of cooling are chosen to be equal. One further parameter is tuned to be the same in both cases. If one assumes that adjacent vertical water columns do not interact, then at any time t, given the surface boundary condition, one can predict the amount of vertically integrated buoyancy content in the water column; which must be equal to the sum of the initial buoyancy content and of the buoyancy removed. Let $I(y, t)$ be the integrated buoyancy content in a ocean of depth H; assuming no lateral transport of buoyancy, one can estimate:

$$I(y, t) = \int_{-H}^{0} b(y, z, t)\, dz = \int_{-H}^{0} b_0(y, z)\, dz + \int_{0}^{t} Q(y, t')\, dt'.$$

The initial conditions and buoyancy fluxes for the preconditioned and localized forcing runs are used to estimate the respective vertically integrated buoyancy $I^p(y, t)$ (for a preconditioned experiment) and $I^l(y, t)$ (for a localized forcing one). This experiment is designed so that at the end of the surface cooling period t_0, $I^p(y, t_0) = I^l(y, t_0)$. Beyond t_0, the two chimneys are allowed to adjust dynamically; if no horizontal processes were active, they would retain the same integrated buoyancy structure beyond t_0.

2) RESULTS

The first comparison is effective in identifying how differences in the initial conditions translate into dif-

TABLE 1. Preconditioned experiments.

Expt	$b_0(y, z)$	N (s^{-1})	L_z (m)	L_y (km)	$Q \times 10^{-7}$ ($m^2\ s^{-3}$)
pre1	$[2 - e^{-(y^2/L_y^2)}]Ne^{z/L_z}$	$N = 3 \times 10^{-4}$	300	15	3.0
pre2	$[N_d - N_g e^{-(y^2/L_y^2)}]e^{z/L_z}$	$N_d = 2N_g = 10^{-3}$	1000	15	3.5
pre3	$[2 - e^{-(y^2/L_y^2)}]Ne^{z/L_z}$	$N = 3 \times 10^{-4}$	300	15	2.57

TABLE 2. Localized forcing experiments.

Expt	$b_0(z)$	N (s^{-1})	L_z (m)	$Q(t, y)$	L_y (km)	$Q_o \times 10^{-7}$ (m^2 s^{-3})
loc1	Ne^{z/L_z}	3×10^{-4}	300	$Q_o e^{-(y^2/L_y^2)}$	15	3.0
loc2	$N_d e^{z/L_z}$	$N_d = 2N_g = 10^{-3}$	1000	$Q_o\left[1 - \frac{N_g}{N_d} e^{-(y^2/L_y^2)}\right]^{-1}$	15	3.5
loc3	$N_d e^{z/L_z}$	$N_d = 2N_g = 10^{-3}$	300	Q_o for $\lvert y\rvert < L_y$	15	2.57

ferently evolving convecting water masses. Figure 2 shows the chimneys formed in experiments pre1 and loc1 overlaid on the respective initial density fields. The choice of parameters causes convection at the center of the chimney to occur to approximately the same depth in both experiments. Because of the different buoyancy fluxes applied, though, the depth of convection at the edge of the chimney strongly varies, thus highlighting one of the major differences: the volume of fluid affected. Because of the different initial conditions, the structure of the cyclonic current is also extremely different (Fig. 2); it is only partially modified by convection in the preconditioned case, leaving an overall stronger and deeper current than ever develops in the localized forcing case. A localized buoyancy flux tends to enhance the density contrast between the region of deepest convection and its surrounding. The opposite is likely to occur in a preconditioned ocean where the same amount of buoyancy is removed everywhere: as the gyre is slowly eroded convection is likely to expose a reduced horizontal gradient. This is shown in Fig. 3, by plotting the time evolution of Δb, the difference in buoyancy measured between fluid at the center of the gyre and fluid 20 km from the center (both taken at a depth of 100 m): $\partial b/\partial y$ (and therefore $\partial \rho/\partial y$) decreases in magnitude in pre1 but increases in loc1. A more detailed discussion of the rate of change of the horizontal gradients is given in section 4. Finally, there is a fairly

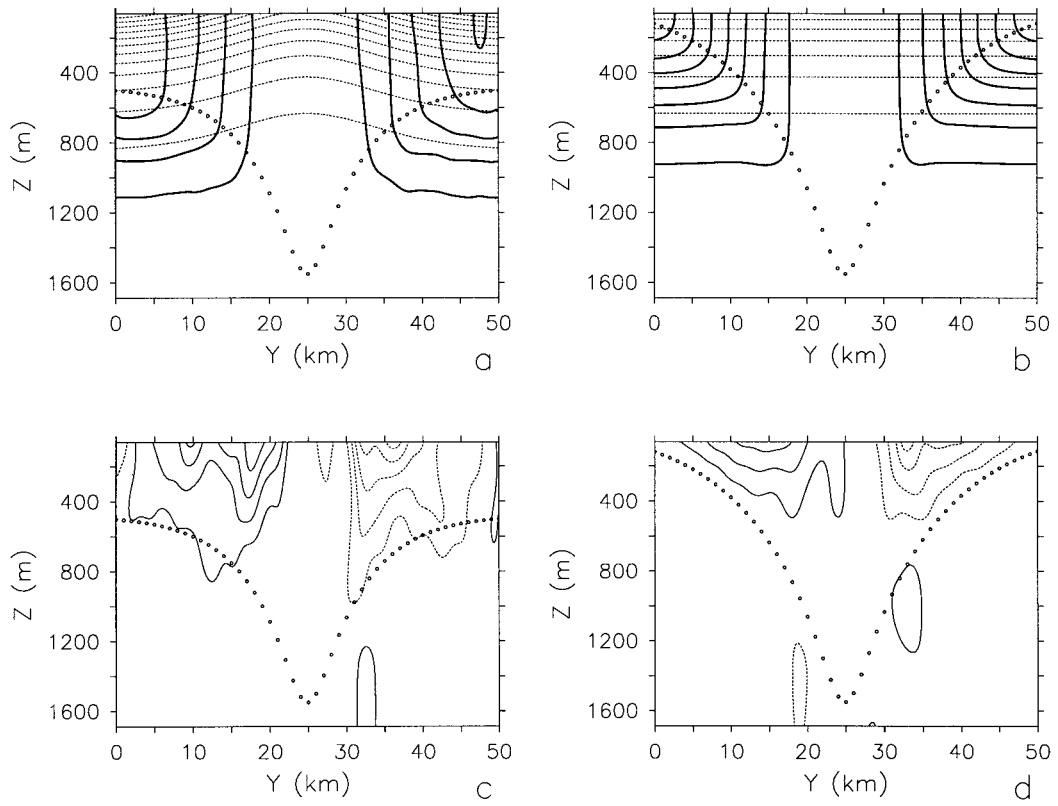

FIG. 2. Initial buoyancy distribution (dashed lines) and final (at day 5) buoyancy distribution (solid lines): (a) pre1 and (b) loc1. Contour interval for the initial condition (4×10^{-5} m s^{-2}) is double that for the final state. Zonal velocity contours at day 5 for (c) pre1 and (d) loc1, contour interval is 2 cm s^{-1}. The mixed layer model depth prediction is superimposed on all (circles).

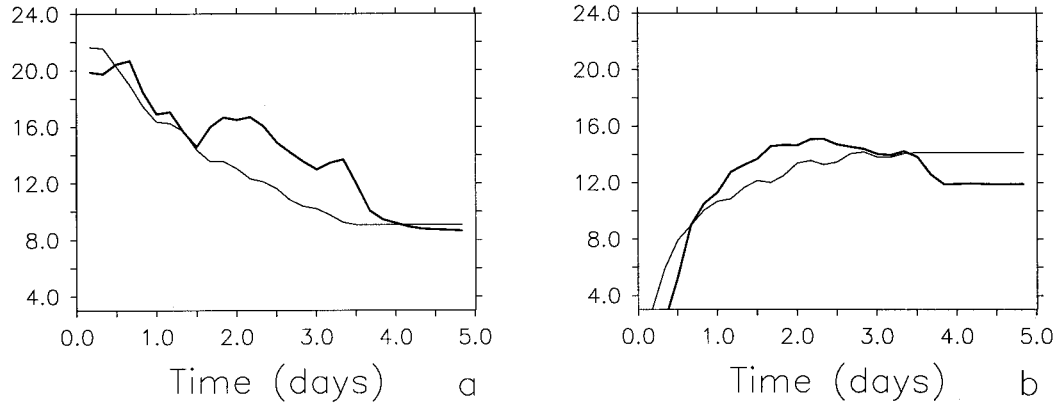

FIG. 3. Evolution of the buoyancy contrast (10^{-5} m s^{-2}) between the edge of the chimney ($y = 5$ km) and its center ($y = 25$ km) measured at 100 m: (a) pre1 and (b) loc1. Thick lines are for the numerical results and thin lines show the mixed layer model prediction.

good agreement between the mixed layer model and the nonhydrostatic model, particularly in predicting the depth of the mixed layer. The discrepancies we observe in the buoyancy distribution can be explained in terms of two aspects of convection that the one-dimensional model does not resolve: a persistent negative stratification while there is a surface buoyancy loss and the geostrophic adjustment of the fluid.

The different density distribution manifests itself in the potential vorticity field for the two chimneys [q as defined in (7)]. A localized buoyancy forcing induces a frontlike potential vorticity structure (Fig. 4) that extends all the way to the surface, to be compared to the almost homogeneous distribution in the top 400 m of the preconditioned experiment and to the overall less pronounced gradient. Finally, the vertically integrated buoyancy $I(y, t_0)$, set to be equal for the two experiments, is in good agreement with the prediction (not shown).

b. Comparison of the same mixed layer depth evolution in time

1) EXPERIMENT DESCRIPTION

Part of the differences between the two cases described above can be traced back to the different volume of fluid involved in the convective overturning. To avoid this problem pre2 and loc2 are designed to have an identical mixed layer depth evolution as predicted by the mixed layer model, the details of which are provided in the appendix. Unlike the other localized forcing experiment presented here, the buoyancy loss must be nonzero everywhere to achieve this (a situation which is very different from the disk of cooling scenario). This condition needs to be met to obtain any mixed layer deepening at all away from the central region and thus be comparable to a preconditioned experiment.

2) RESULTS

There is a greater similarity between these two runs than the previous ones, mostly because the volume of fluid affected is the same for both. Equal *mixed layer depth*, though, does not necessarily imply similar chimneys, as shown in Fig. 5. Because the preconditioning vorticity in pre2 extends to a much greater depth than that reached by convection, its horizontal density gradient is almost unmodified (Fig. 6a), to be contrasted with the small gradient in the localized forcing experiment (Fig. 6b). These features are reflected in the rim current's intensity and shear (Fig. 5). We do not show the potential vorticity distribution since it can be inferred from the buoyancy fields shown in Fig. 5; however, it is worth pointing out that its horizontal and vertical gradients are larger for the localized forcing case, where isopycnals have to flatten and become horizontal over a small distance compared to the doming ones in pre2.

c. Comparison of two cases with the same rate of buoyancy removed

1) EXPERIMENT DESCRIPTION

We take the opportunity of this last comparison to use the *disk of cooling* forcing, which has almost always been used in previous simulations of localized convection (Jones and Marshall 1993; Maxworthy and Narimousa 1994; and others), and choose the rate of buoyancy removed as the quantity to set equal. Three experiments are discussed here: loc3, pre3, and loc1, the last being from the first set of comparisons. In loc3 a constant buoyancy flux $Q = \overline{Q}(t)$ is applied within a limited region and no buoyancy is removed elsewhere; the same buoyancy flux is removed over the whole model domain in pre3. The value of this buoyancy flux is chosen to be equal to the mean buoyancy flux applied in loc1, defined as

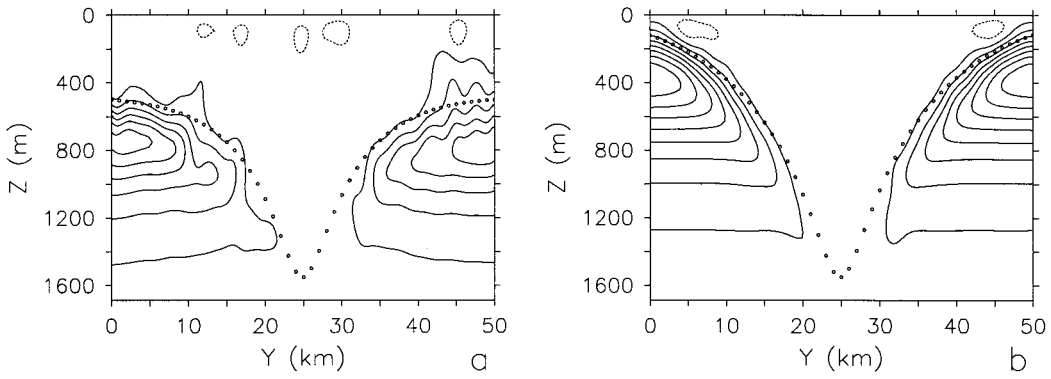

FIG. 4. Potential vorticity at day 5 for (a) pre1 and (b) loc1. Contour interval is 3×10^{-12} s^{-3}. Overlayed is the mixed layer model prediction for the depth of convection (circles).

$$\overline{Q}(t) = \frac{1}{2L_f} \int Q(y, t)\, dy,$$

where the integral is over the model domain and L_f is the *e*-folding length of the Gaussian function used in loc1. The background stratification is the same for all experiments and the time dependence of the buoyancy flux is also chosen to be identical; details of the experiments are given in Tables 1 and 2.

2) RESULTS

Figure 7 shows some of the features inherent to the *disk of cooling forcing*: a horizontally homogeneous convected water mass with narrow boundary regions at the edge where the potential vorticity front, the density front, and the geostrophic velocity are concentrated. The width of these regions must be of the order of the deformation radius of the unmodified fluid, as suggested

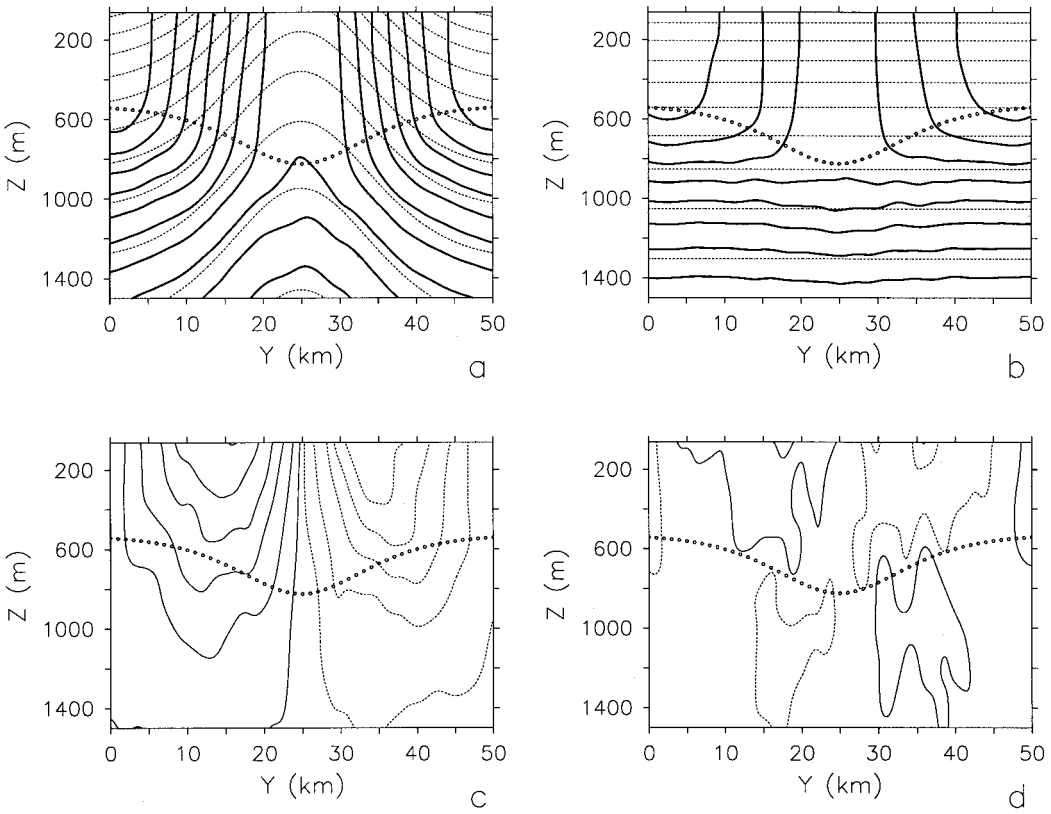

FIG. 5. Initial buoyancy distribution (dashed lines) and final (at day 5) buoyancy distribution (solid lines) for (a) pre2 and (b) loc2. Contour interval for the initial condition (4×10^{-5} m s^{-2}) is double that for the final state. Zonal velocity contours at day 5 (c) pre2 and (d) loc2, contour interval is 4 cm s^{-1} in (c) and 2 cm s^{-1} in (d). The mixed layer model depth prediction is superimposed on all (circles).

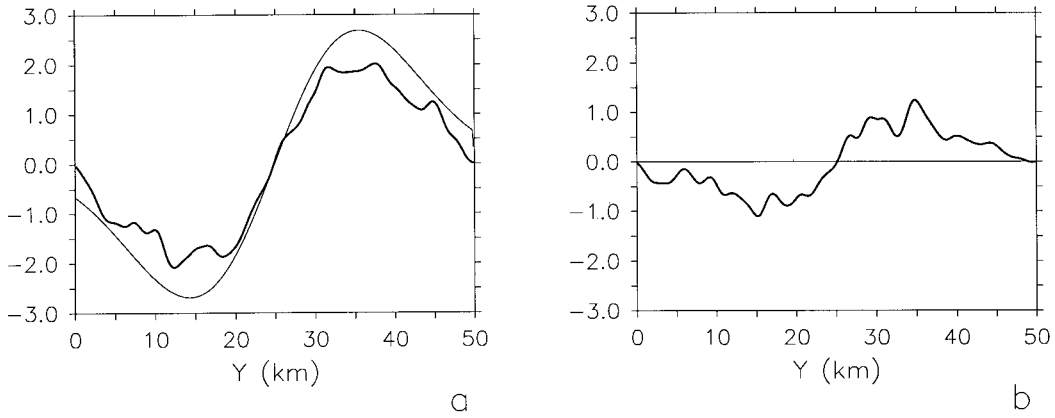

FIG. 6. Horizontal buoyancy gradient (10^{-8} s^{-2}) at 100 m showing the initial condition (thin) and the final state (solid) for (a) pre2 and (b) loc2.

in numerous localized forcing studies. Similarly, the interior convected region has no horizontal density structure because of the absence of gradients both in the forcing or in the initial conditions. If we compare these features to those obtained in loc1 (Fig. 2) we can see that the gradients within and at the edges of the chimney in the disk of cooling forcing are much stronger. This shows how the structure of the chimney is greatly influenced by the shape of the forcing. Figure 7 also shows a section of the chimney formed in pre3: the frontal region is much weaker in this preconditioned experiment compared with the sharp one in loc3 and the smoother one of loc1.

This last comparison illustrates the sensitivity of the

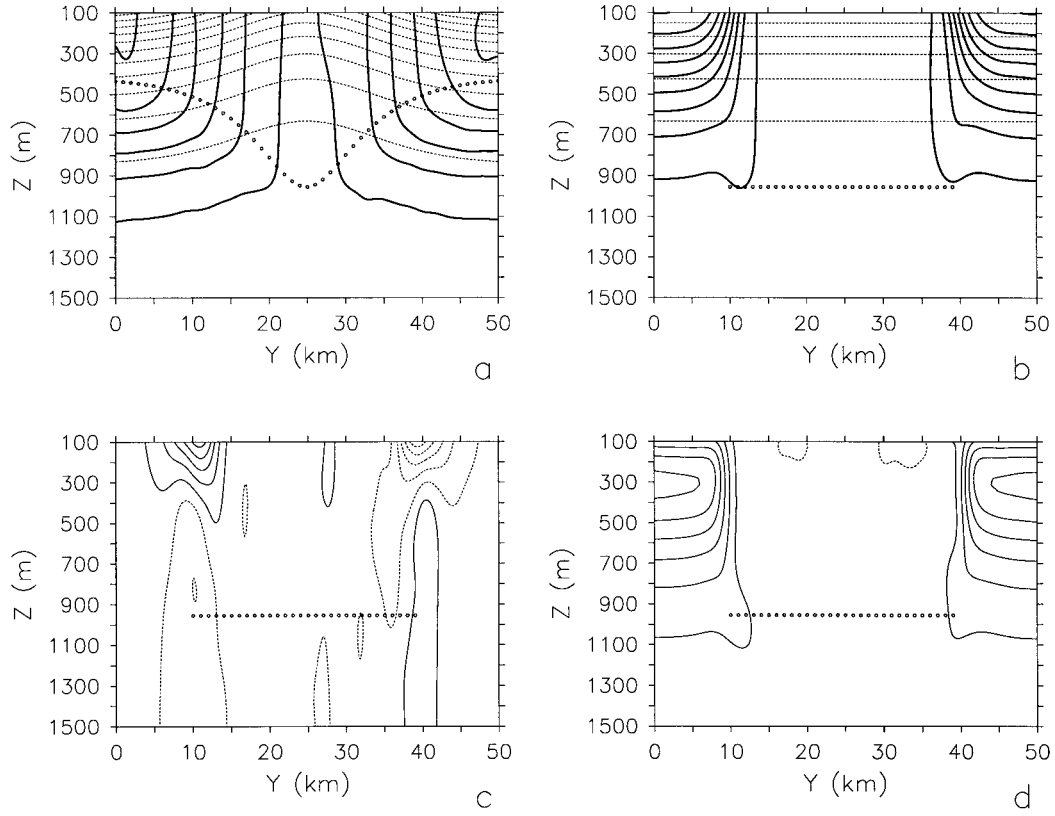

FIG. 7. Initial buoyancy distribution (dashed) and final (at day 5) distribution (solid) for (a) pre3 and (b) loc3. Contour interval of the initial state (4×10^{-5} m s^{-2}) is double that of the final state. Overlayed is the mixed layer model prediction for the mixing depth (circles). (c) Zonal velocity for loc3, contour interval is 2 cm s^{-1} at day 5 (d) potential vorticity for loc3, contour interval is 5×10^{-12} s^{-3}, day 5.

chimney formed to the shape and magnitude of the buoyancy forcing and confirms some of the findings of the previous comparisons. First, there is no simple way of designing a localized forcing simulation so that the chimney produced is similar to one produced during preconditioned convection. Moreover, some features of the convected fluid are not common to both scenarios and, in particular, localized forcing tends to enhance the frontal region at the edge of the chimney inducing an increase in the horizontal density gradient. The evolution of this gradient is the focus of the following section.

4. Rate of change of the horizontal density gradient during convection

The horizontal density gradient within and at the edge of a chimney allows for storage of available potential energy that can, in turn, support the development of baroclinic instability. Thus, knowledge of its evolution is relevant to all questions regarding the chimney's collapse and export of dense water from the region of formation. In comparing experiments pre1 and loc1, we showed that the horizontal density gradient's evolution can differ for the two convective scenarios (Fig. 3): It decreases in the preconditioned experiment but increases in the localized forcing one. In this section we explain this result and argue that it is valid for a more general class of preconditioned and localized forcing scenarios.

a. Localized forcing scenario

Consider the disk of cooling scenario: Fluid below the active buoyancy forcing will become denser in time as cooling persists, whereas fluid outside the forced region will retain its initial density until baroclinic processes become active. As a result the density difference between the region of convection and the external region can only *increase* in time, leading to a growing frontal structure between convected and unmodified fluid. The disk of cooling scenario is a special case of a spatially variable surface buoyancy loss, with zero buoyancy flux in the region outside the disk. Consider now the case of a continuous but horizontally varying surface buoyancy loss [i.e., $Q = Q(y, t)$] where the rate of change of the horizontal density gradient can be diagnosed with the help of the one-dimensional mixed layer model making use of (2). If the initial density field is horizontally homogeneous, the conservation equation becomes

$$\overline{b}(y, t)h(y, t) - \int_{-h(y,t)}^{0} b_0(z)\, dz = \int_0^t Q(y, t')\, dt', \quad (8)$$

where $\overline{b}$ is defined in section 2a(1). As a simplification we assume that the buoyancy forcing is constant in time once it is turned on, that is, $\int_0^t Q(y, t')\, dt' = Q(y)t$. We can then differentiate (8) with respect to y and, provided the mixed layer depth is nonzero,

$$\frac{d\overline{b}}{dy} = \frac{dQ}{dy}\frac{t}{h(y, t)}. \quad (9)$$

Consider the time evolution of the horizontal density gradient by differentiating with respect to time:

$$\frac{d\overline{b}_y}{dt} = \frac{dQ}{dy}\frac{1}{h(y, t)}\left(1 - \frac{t}{h}\frac{dh}{dt}\right) \quad (10)$$

and let

$$R_l = \left(1 - \frac{t}{h}\frac{dh}{dt}\right).$$

The horizontal density gradient will increase or decrease in time depending on the sign of R_l. In other words, the sign of the horizontal density gradient depends on the rate of growth of the mixed layer in time: If the mixed layer depth h grows at a rate linearly proportional to time, then $d\overline{b}/dy$ remains constant in time; if the rate of growth is faster, the horizontal density gradient decreases; and if the rate is slower, it increases. To examine how (10) works, we examine the sign of R_l for two simple cases of background stratification. First, consider the case of a stably stratified ocean of the form $b_0(z) = -A|z|^\alpha$, with $\alpha > 0$ and A a positive constant. For any α such that $0 < \alpha < 1$, it represents an ocean where stratification is maximum at the surface, whereas for $\alpha > 1$, stratification increases with depth. By solving (8), it is straightforward to derive the mixed layer depth, $h(y, t) = ct^{1/(1+\alpha)}$, where c is a positive constant, $c = \{-(\alpha + 1)Q/[(\alpha + 2)A]\}^{1/(1+\alpha)}$. The sign of $d\overline{b}_y/dt$ from (10) is determined by the sign of R_l, substituting $h = ct^{1/(1+\alpha)}$:

$$R_l = \left(1 - \frac{t}{h}\frac{dh}{dt}\right) = 1 - \frac{1}{1 + \alpha} > 0 \quad \text{for every } \alpha > 0.$$

This shows that for this form of background stratification (the linear background stratification being a special case with $\alpha = 1$) $\overline{b}_y$ will always increase in time as long as the cooling persists.

Consider now the case of an exponential background stratification, decaying away from the surface: $b_0(z) = b_o e^{z/H}$. The exact same calculations as above lead to

$$R_l = 1 + \frac{H(H + h - He^{h/H})}{h^2}.$$

As the mixed layer is penetrating the uppermost stratified fluid, R_l is positive leading to an increase in the horizontal density gradient. Once convection has reached beyond this upper layer as the fluid becomes less and less stratified, R_l changes sign (when $t \approx 0.55b_0 H/Q$). Convection within this almost unstratified fluid leads to a change in sign in R_l, which is associated with a weakening horizontal density gradient. If con-

vection persists, the mixed layer depth h grows to a logarithmic singularity at $t = b_0H/Q$ representing convection in a vertically unstratified fluid.

Thus, there are a number of cases of localized forcing convection (including that of a linearly stratified fluid) where the horizontal density gradient will increase as convection occurs leading to a growing frontal structure at the edge of the deep convection. In particular, this must be true of the disk of cooling experiment. The parameter that governs the rate of growth of the horizontal density gradient is the rate of mixed layer deepening as a function of time. Our calculations for an exponentially decaying stratification show that the increase in the horizontal density gradient occurs at least in the initial stages of convection, when it is eroding a stratified fluid. Once the stratification is eroded, there is nothing to support the horizontal gradients and the fluid tends to become homogeneous. However, it should be pointed out that (10) only measures the rate of change of $d\overline{b}/dy$ in time at one particular location. Seen globally, the region with the largest horizontal density gradient (i.e., the chimney's edge) propagates away from the center in time. Thus, the region of enhanced horizontal gradient would persist at the edge of the chimney so long as the chimney remains finite in horizontal extent.

b. Preconditioned scenario

Consider now the case of a preconditioned ocean with a uniform buoyancy loss Q at the surface (y independent). Following the procedure for the localized forcing scenario, we can simplify (2) to

$$\overline{b}(y, t)h(y, t) - \int_{-h}^{0} b_0(y, z)\, dz = Qt, \qquad (11)$$

and differentiating with respect to y,

$$\frac{\partial \overline{b}}{\partial y} = \frac{1}{h}\int_{-h}^{0} \frac{\partial b_0}{\partial y}\, dz; \qquad (12)$$

that is, the horizontal density gradient is a vertical average of the horizontal density gradient of the initial stratification over the depth of the mixed layer depth. It can be easily inferred from (12) that if the magnitude of the horizontal density gradient increases in z (i.e., the gyre is surface intensified) then the horizontal density gradient must *decrease* with a deepening mixed layer. More explicitly, if we take the time derivative of (12),

$$\frac{d\overline{b}_y}{dt} = -\frac{1}{h}\frac{dh}{dt}\left(\frac{1}{h}\int_{-h}^{0} \frac{\partial b_0}{\partial y}\, dz - \frac{\partial b_0}{\partial y}(y, -h)\right), \qquad (13)$$

and let

$$R_p = \left(\frac{1}{h}\int_{-h}^{0} \frac{\partial b_0}{\partial y}\, dz - \frac{\partial b_0}{\partial y}(y, -h)\right).$$

Since the mixed layer must grow in time, the horizontal density gradient will increase in time if R_p is less than zero or decrease for R_p greater that zero, where R_p is the difference between the vertical average of the horizontal density gradient, averaged over a depth equal to the mixed layer depth, and the actual value of the horizontal density gradient at that depth of the initial preconditioned ocean. If the preconditioning is surface intensified and decays with depth, it follows that the average over any depth h will always be larger than the value at h, and therefore R_p is always positive. For this case, the horizontal density gradient must decrease in time. On the other hand, if the preconditioning structure intensifies with depth, the horizontal density gradient must increase as a result of convection. Finally, the evolution of the horizontal density gradient will vary for any case of middepth intensified preconditioning.

Deep convection in the ocean typically occurs in regions of surface stratification overlying deeper weakly stratified fluid. These calculations show that, for this situation, the horizontal density gradient will continuously decrease as a result of convection, extending the result shown in Fig. 3 to the more general case of horizontal stratification decreasing with depth. They also imply that the absence of horizontal gradients observed in oceanic chimneys (e.g., by Leaman and Schott 1991, in the northwest Mediterranean) does not necessarily require any horizontal mixing, instead it can result from convection into deeper layers, exposing a horizontally homogeneous water mass.

c. Summary

These calculations have shown that, in time, the horizontal density gradient in a preconditioned convection scenario can evolve in the opposite direction from that of a localized forcing case. We have identified a number of localized forcing cases where this gradient increases in time during a convective event (among these is the disk of cooling) and then argued that for any preconditioned case in which the preconditioning is surface intensified, the gradient must decrease. Although these calculations are limited to a one-dimensional mixing argument, our numerical experiments show that they also hold for two-dimensional convection. Moreover, a number of numerical and laboratory experiments have shown the one-dimensional mixed layer prediction to hold until the onset of baroclinic instability. It is therefore reasonable to assume that these calculations also apply to a more general, three-dimensional case. The implications of this result are discussed in the next section.

5. Discussion

Our present knowledge of localized deep convection in the ocean has derived from a series of laboratory and numerical experiments in which the more realistic case of convection in a preconditioned ocean is replaced by

a simpler-to-model case of localized convection due to a localized forcing: both scenarios result in the formation of a localized body of dense water. Although we have undoubtedly benefited from these simulations, little attention has been paid to what the limitations of this substitution are and to whether results derived from a localized forcing case also apply to a preconditioned one.

In comparing the two scenarios, the first difficulty we encountered was that of defining an equivalence between the two. In one case the horizontal scale of the volume of fluid affected by the buoyancy loss is fixed in time and determined by the surface boundary condition, whereas in the other case the horizontal scale evolves as a function of the variation of the preconditioning structure with depth given by the initial condition. Consequently, there is no simple translation of the governing parameters for one case to the other. Indeed, the number of parameters that define preconditioned convection is greater than those defining locally forced convection. This makes it difficult to extend the scaling laws and parameterizations derived for the localized forcing scenario, for example, by Jones and Marshall (1993) and expanded by Send and Marshall (1995), directly to the preconditioned scenario.

Of the differences we found, the most important one concerns the different evolution of the horizontal density gradient for the two scenarios. Numerical and analytical calculations confirm that, while the horizontal density gradient between the deep convection region and the surroundings must increase in time in a localized forcing scenario, this same gradient will decrease in a preconditioned ocean in which the preconditioning decays with depth. This gradient, both in density and potential vorticity, supports the growth of baroclinic instability which has been shown to be the dominating mechanism in the collapse of the chimney and the advection of dense water away from its formation site. Although this breakdown mechanism, identified in the localized forcing scenarios, is likely to play a role in the preconditioned case too, as Legg et al.'s (1998) experiments indicate, it is reasonable to speculate that the growth rate of the instability and its effectiveness will be different.

Consider, for example, the result that baroclinic instability can halt the growth of a chimney. This arrest of the deepening of the chimney has been observed in the numerical experiments of Legg and Marshall (1993) and Visbeck et al. (1996) and in the laboratory experiments of Ivey and Coates (1995). The theoretical explanation is discussed in Visbeck et al. (1996): a chimney can reach a steady state even with an active buoyancy loss if the eddy fluxes balance the surface buoyancy loss. Visbeck et al. derive a parameterization of the eddy fluxes ($\overline{v'b'}$) based on the density contrast between the convected fluid and the unmodified neighboring ocean,

$$\overline{v'b'} = \alpha \frac{\overline{b'^2}}{N},$$

and verify its validity in a number of numerical and laboratory simulations. Because the density contrast must increase in a localized forcing scenario, it follows that the eddy flux must also increase in time. There will always be a final time then, t_{final} in Visbeck et al., when it has grown sufficiently to match the (constant) surface buoyancy loss. For this reason, in a localized forcing experiment, one can find an equilibration depth for the chimney beyond which the mixed layer ceases to grow and the heat removed at the surface is balanced by a heat flux in due to the baroclinic eddies. Consider this same argument applied to a preconditioned ocean and suppose that the eddy flux can still be parameterized as a function of the square of the density gradient: because this decreases in time, the associated eddy flux must also decrease in time. This appears to suggest that no equilibrium state of the type observed for a chimney due to localized forcing is possible. Although we do not believe that the chimney can deepen indefinitely (and the results of Legg et al. 1998, confirm our belief), the parameterization of the fluxes due to the baroclinic eddies derived for the localized forcing scenario suggest that it may. This is an example of how results derived in the localized forcing scenario may not apply to a preconditioned ocean.

Finally, the differences between the nonhydrostatic model and the one-dimensional mixing model can typically be accounted for in terms of two processes that the one-dimensional mixing model cannot resolve: geostrophic adjustment and a persistent, unstable stratification in the surface boundary layer while there is a surface buoyancy loss. These results indicate that, until the development of baroclinic instability, convection is essentially a vertical mixing process and that no other two-dimensional process appears to play a significant role in the redistribution of fluid during convection. This is in contrast with the suggestion made by Legg et al. (1998) and Haine and Marshall (1998) that symmetric instability (also known as slantwise convection) is responsible for the partial restratification of the water column during convection. No restratification is observed in our simulations during active convection, and regions of negative potential vorticity are typically associated with either an unstable vertical stratification or with patches of centrifugally unstable fluid around the plumes and on the plume scales. Since the nonhydrostatic model is fully capable of resolving symmetric instability, we can only conclude that it did not play a significant role in our experiments. This indicates that convection (either in localized forcing experiments or in preconditioned ones) is not always able to generate symmetrically unstable flow. The role played by symmetric instability in restratifying the water column must then be investigated further by analyzing a greater range of preconditioning structures with differing horizontal density gradients.

6. Conclusions

We have compared deep overturning in the presence of a preconditioning cyclonic region to that due to a spatially localized cooling. The motivation is given by the widespread use of localized forcing experiments to simulate deep, localized convection. In a series of comparisons, we have found that there are some fundamental differences in the evolving density fields even when the parameters are tuned to be as close as possible, the main one being the different evolution of the horizontal density gradient. Since baroclinic instability is dependent on the existence of such a gradient, the implication is that a chimney formed in a preconditioned ocean will not evolve in the same manner as one formed as a result of a localized buoyancy loss after the onset of baroclinic instability. In particular, we have argued that it is unlikely that a chimney formed in a preconditioned ocean will reach an equilibrium state where the surface buoyancy loss is balanced by a lateral eddy flux, a result often observed in localized forcing simulations.

While we believe that knowledge of oceanic convection can still benefit from localized forcing simulations, our calculations and experiments indicate a need to be aware of the limitations of such a scenario. The localized forcing approach has proven to be valid in identifying the physical processes occurring during localized convection, such as the plumes and the chimney breakup as a result of baroclinic instability. However, more realistic simulations of preconditioned convection are needed to quantify these processes if the goal is to include parameterized convection in the larger-scale models.

Acknowledgments. This work originated from FS's participation in the Geophysical Fluid Dynamics Summer School on Rotating Convection held at Woods Hole in 1995 and has benefited from numerous discussions with all the people present at Walsh Cottage and, in particular, with Glenn Flierl and John Marshall. We would like to thank Sonya Legg and Al Hermann for helpful discussions, LuAnne Thompson for proofreading the manuscript, and Steve Riser for continuous support. Most of the figures in this paper were produced using FERRET, an interactive gridded data package developed by Steve Hankin, and others, at PMEL. This work was supported by the Office of Naval Research Grant N00015-95-J-1307 and the National Science Foundation Grant Oce 9302082 and Oce 9311550.

APPENDIX

Description of the Two Experiments with the Same Mixed Layer Depth

Experiments loc2 and pre2 are designed to have the same mixed layer depth at any time according to the mixed layer model, presented in section 2a(1). Using the buoyancy conservation equation (2) one can construct a preconditioned and a localized forcing experiment where the equation for $h(y, t)$ is identical, without explicitly needing to solve for $h(y, t)$. Consider a simple preconditioning experiment where the initial buoyancy distribution $b_0(y, z) = \hat{b}_p(z) f(y)$ and where the surface buoyancy loss $Q(y, t) = B_0 t$. Equation (2) then reduces to

$$\hat{b}_p(-h) f(y) h(y, t) - f(y) \int_{-h}^{0} \hat{b}_p(z)\, dz = B_0 t, \quad \text{(A1)}$$

which provided $f(y)$ is nonzero, can be written in the form

$$\hat{b}_p(-h) h(y, t) - \int_{-h}^{0} \hat{b}_p(z)\, dz = \frac{B_0 t}{f(y)}. \quad \text{(A2)}$$

Similarly for the localized forcing case, let the initial conditions be $b_0(z) = \hat{b}_l(z)$ and the surface buoyancy flux be of the form $Q(y, t) = B_0 g(y) t$, Eq. (2) then becomes

$$\hat{b}_l(-h) h(y, t) - \int_{-h}^{0} \hat{b}_l(z)\, dz = B_0 g(y) t. \quad \text{(A3)}$$

For h to be identical, for every y and every t, for both cases then the equation for h must be the same for both. This implies choosing $\hat{b}_l = \hat{b}_p$, removing the same magnitude buoyancy flux and having $g(y) = 1/f(y)$; that is, the spatial dependence of the forcing in the localized forcing experiment must be the same as the reciprocal of the function modulating the preconditioning in the horizontal direction (see Tables 1 and 2).

REFERENCES

Alverson, K., and W. B. Owens, 1996: Topographic preconditioning of open-ocean deep convection. *J. Phys. Oceanogr.,* **26,** 2196–2213.

Bryden, H., 1993: Ocean heat transport across 24°N latitude, *Interactions between Global Climate Subsytems,* G. A. McBean and M. Hantel, Eds., Vol. 15, IUGG, 65–75.

Gascard, J. C., and R. A. Clarke, 1983: The formation of Labrador Sea water. Part II: Mesoscale and smaller-scale processes. *J. Phys. Oceanogr.,* **13,** 1779–1797.

Haine, T., and J. Marshall, 1998: Gravitational, symmetric and baroclinic instability of the ocean mixed layer. *J. Phys. Oceanogr.,* **28,** 634–658.

Hermann, A., and B. Owens, 1993: Energetics of gravitational adjustment for mesoscale chimneys. *J. Phys. Oceanogr.,* **23,** 346–371.

Hogg, N. G., 1973: The preconditioning phase of MEDOC 1969-II. Topographic effects. *Deep-Sea Res.,* **20,** 449–459.

Ivey, G. H., and M. Coates, 1995: Convectively driven mixed layer growth in a rotating, stratified fluid. *Deep-Sea Res.,* **42,** 331–349.

Jones, H., and J. Marshall, 1993: Convection with rotation in a neutral ocean: A study of open-ocean deep convection. *J. Phys. Oceanogr.,* **23,** 1009–1039.

——, and ——, 1997: Restratification after deep convection. *J. Phys. Oceanogr.,* **27,** 2276–2287.

Leaman, K., D. and F. A. Schott, 1991: Hydrographic structure of

the convection regime in the Gulf of Lions: Winter 1987. *J. Phys. Oceanogr.*, **21,** 575–595.

Legg, S., and J. Marshall, 1993: A heton model of the spreading phase of open-ocean deep convection. *J. Phys. Oceanogr.*, **23,** 1040–1056.

——, H. Jones, and M. Visbeck, 1996: A heton perspective of baroclinic eddy transfer in localized ocean deep convection. *J. Phys. Oceanogr.*, **26,** 2251–2266.

——, J. McWilliams, and J. Gao, 1998: Localization of deep ocean convection by a mesoscale eddy. *J. Phys. Oceanogr.*, **28,** 944–970.

Madec, G., F. Lott, P. Delecluse, and M. Crepon, 1996: Large-scale preconditioning of dense-water formation in the northwestern Mediterranean *J. Phys. Oceanogr.*, **26,** 1393–1408.

Maxworthy, T., and S. Narimousa, 1994: Unsteady, turbulent convection into a homogeneous, rotating fluid, with oceanographic applications. *J. Phys. Oceanogr.*, **24,** 865–887.

Muench, R. D., 1988: Relict convective features in the Weddell Sea. *Deep Convection and Deep Water Formation in the Oceans*, P. C. Chu and J. C. Gascard, Eds., Elsevier, 53–67.

Schott, F., M. Visbeck, and J. Fischer, 1993: Observations of vertical currents and convection in the central Greenland Sea during the winter of 1988/89. *J. Geophys. Res.*, **98,** 14 401–14 421.

Send, U., and J. Marshall, 1995: Integrals effects of deep convection. *J. Phys. Oceanogr.*, **25,** 855–872.

Swallow, J. C., and G. F. Caston, 1973: The preconditioning phase of MEDOC 1969-I. *Deep-Sea Res.*, **20,** 429–448.

Visbeck, M., J. Marshall, and H. Jones, 1996: Dynamics of isolated convective regions in the ocean. *J. Phys. Oceanogr.*, **26,** 1721–1734.